Florence, Italy 12-16 July 2015
ICSV22
The 22nd International Congress on Sound and Vibration

HELMHOLTZ RESONATORS FOR DAMPING COMBUSTOR THERMOACOUSTICS

Dong Yang and Aimee S. Morgans
Department of Aeronautics, Imperial College London, London, UK, SW7 2AZ
email: d.yang13@imperial.ac.uk

Helmholtz resonators (HRs) are commonly used to damp thermoacoustic oscillations in gas turbine combustors. In practice the HR is often maintained at a cooler temperature than the combustor, but this tends to be neglected when modelling. In the first part of this work, we derive an analytical model for both the acoustic damping and the effect on the combustor of HRs whose volume is at a different temperature to the combustor. The energy conservation equation based on the stagnation enthalpy, together with the mass and momentum conservation equations, is incorporated into a linear HR sound absorption model. These are coupled with linear wave-based models for the plane acoustic waves in the combustor. The temperature difference is found to generate an entropy wave which advects downstream of the resonator (and may generate further acoustic waves if accelerated), and to change the acoustic damping near the resonant frequency. We then go on to consider using multiple HRs to achieve wide bandwidth sound absorption, via tuning the HRs to slightly offset frequencies. We consider two methods for optimising the HR positions within the combustor. The performance of the multiple HRs are then tested in an open source combustion instability low order simulator (OSCILOS).

1. Introduction

Helmholtz resonators are widely used as passive dampers for their simple structure and their robust acoustic absorption performance.[1] A typical Helmholtz resonator consists of a small neck opening to a large chamber. Small pressure perturbations at the neck mouth give rise to large mass flux oscillations in the neck at resonance. This resonant frequency can be predicted by the common model (which does not account for acoustic damping) $f_{\text{ref}} = c/(2\pi)\sqrt{S/(Vl)}$, where c is sound velocity in the chamber, S, l, V are neck cross-sectional area, neck length, and chamber volume respectively. To account for the acoustic damping of the resonator, nonlinear and linear models are generally used for cases without and with a mean neck flow (also called a bias flow) respectively. In the absence of a neck mean flow, energy absorption is usually related to the nonlinear viscous damping of the flow in the neck region which is captured by a nonlinear model such as proposed by Cummings.[2] This model has been successfully validated and used by many researchers.[3–5] In the presence of a mean bias flow, incident acoustic waves cause unsteady vortices to be shed at the edges of the neck apertures, which are swept away by the mean flow. The local absorption is characterized by the Rayleigh conductivity.[6]

When a HR is attached to a real combustor, a bias cooling flow is typically needed to protect the HR from being damaged by the high temperature in the combustor. Both steady and oscillating

cold fluxes are then injected from the neck into the combustor. As the mean mass flux from the HR is generally much smaller than the mean flow within the combustor, the mean flow changes slightly across the HR. The oscillating neck mass flux, however, may be of the same order as that in the combustor near the resonant frequency, making mixing of this oscillating cold flow and the hot flow in the combustor critical in predicting the relations between oscillations before and after the HR. It is worth noting that the effect of hot-gas penetration in the neck of the resonator at large oscillation amplitudes has been found to alter the sound absorption performance of the HR.[7] In low-order network model, it is more interesting to know how the HR affects the acoustic (and entropy) waves in the combustor, which was not considered in the previous study. By incorporating a stagnation enthalpy based energy conservation equation into a linear wave-based model for plane acoustic waves in the combustor, it is shown in the next section that an entropy wave is generated after the HR and the relation between acoustic waves before and after the HR is also changed compared to the case in which the temperature difference is neglected. This impact (entropy generation and acoustic wave changes) occurs whenever the temperature of the injected flow from the neck is different from that in the combustor, weather a linear or a nonlinear HR damping model is used.

As a HR responds only to pressure oscillations at its entrance, its location along the pressure modeshape is critical to its damping performance at the relevant frequency.[4] Combustors may exhibit unstable modes of different frequencies depending upon operating conditions, and a HR tuned to a specific resonant frequency will have limited absorption bandwidth. One possible way of extending the bandwidth is to use multiple HRs, each tuned to a different frequency. In order to provide acoustic damping for all modes in a given frequency range, it may be attractive to maintain a certain sound absorption coefficient over a given bandwidth. As a HR changes the modeshape within the combustor, an optimization procedure to choose the axial distribution of these HRs is necessary. Gradient- and modeshape-based methods are presented in this article to optimize the HR locations of a multi-HR combustor. The performance is validated by applying the resonators in an open source combustion instability low order simulator (OSCILOS).

2. The impact of a cold HR cavity on the combustor thermoacoustics

When a HR is attached to a combustor, as shown in Fig. 1, the flow parameters before (denoted by subscript $_1$), after (denoted by subscript $_2$) the resonator and at the resonator neck (denoted by subscript $_n$) can be related by using the conservation relations.

$$m_2 = m_1 + m_n, \quad f_2 = f_1, \quad e_2 = e_1 + e_n, \tag{1}$$

where $m,\ f,\ e$ denote mass, axial momentum and energy flux, respectively. Here we express all flow variables as the sum of a mean ($\bar{}$) and fluctuating ($\widetilde{}$) component (for example, $m = \bar{m} + \widetilde{m}$). The momentum in the x-direction is constant because the neck flow is assumed to be radially inwards within the combustor. Considering mean flow, Eq. (1) can be written as

$$\begin{aligned} &\bar{\rho}_2\bar{u}_2 = \bar{\rho}_1\bar{u}_1 + \bar{\rho}_n\bar{u}_n\frac{S_n}{S_c}, \quad \bar{p}_2 + \bar{\rho}_2\bar{u}_2^2 = \bar{p}_1 + \bar{\rho}_1\bar{u}_1^2, \\ &\bar{\rho}_2\bar{u}_2(C_{p2}\bar{T}_2 + 0.5\bar{u}_2^2) = \bar{\rho}_1\bar{u}_1(C_{p1}\bar{T}_1 + 0.5\bar{u}_2^2) + \bar{\rho}_n\bar{u}_n\frac{S_n}{S_c}(C_{pn}\bar{T}_n + 0.5\bar{u}_n^2), \end{aligned} \tag{2}$$

where C_p denotes heat capacity at constant pressure, which is a function of the temperature and the ideal gas relation gives $\bar{p} = \bar{\rho}R\bar{T}$. Given $\bar{\rho}_1$, $\bar{u}_1$ and $\bar{T}_1$, $\bar{\rho}_2$, $\bar{u}_2$ and $\bar{T}_2$ can be calculated from Eqs. (2). The mass, momentum and energy conservation equations can then be considered for fluctuations, retaining only linear contributions to give

$$\widetilde{m}_2 = \widetilde{m}_1 + \widetilde{m}_n, \quad \widetilde{f}_2 = \widetilde{f}_1, \quad \widetilde{e}_2 = \widetilde{e}_1 + \widetilde{e}_n. \tag{3}$$

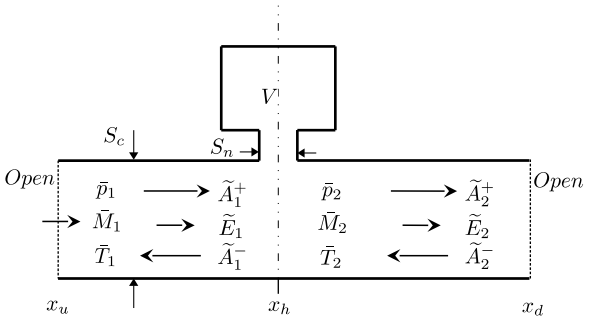

Figure 1: A Helmholtz resonator installed in an acoustic duct (combustor).

where $\widetilde{e}_n = \bar{B}_n\widetilde{m}_n + \bar{m}_n\widetilde{B}_n$ denotes the energy flux oscillation from the resonator into the combustor. $\bar{B}_n = C_{pn}\bar{T}_n + 0.5\bar{u}_n^2$ is the mean neck stagnation enthalpy, with $\widetilde{B}_n$ the oscillation. An acoustic model of the HR is included to relate $\widetilde{m}_n$ to the pressure oscillations at the HR entrance. A linear model based on the Rayleigh conductivity[6] is used, with $\widetilde{m}_n$ related to the entrance pressure by

$$\widetilde{p}_{x_h} = -\left(\frac{\bar{c}_v^2}{i\omega V} + \frac{i\omega}{K'_R}\right)\widetilde{m}_n, \tag{4}$$

where $\widetilde{p}_{x_h}$ is the oscillating pressure at the HR entrance, V and $\bar{c}_v$ are the cavity volume and sound speed, ω is angular frequency and K'_R is the revised Rayleigh conductivity defined in references[8–10] which accounts for the finite length of the HR neck. Mass, momentum and energy flux perturbations in the combustor can be related to the downstream ($\widetilde{A}^+$) and upstream ($\widetilde{A}^-$) travelling acoustic wave strengths and entropy ($\widetilde{E}$) wave strength by

$$[\widetilde{m}(x), \widetilde{f}(x), \widetilde{e}(x)]^T = \boldsymbol{M_{w2f}}[\widetilde{A}^+(x), \widetilde{A}^-(x), \widetilde{E}(x)]^T, \tag{5}$$

where the wave to flux transfer matrix is

$$\boldsymbol{M_{w2f}} = S_c \begin{bmatrix} \frac{\bar{M}+1}{\bar{c}} & \frac{\bar{M}-1}{\bar{c}} & \frac{-\bar{M}}{\bar{c}} \\ (\bar{M}+1)^2 & (\bar{M}-1)^2 & -\bar{M}^2 \\ \bar{c}\left(\frac{\gamma\bar{M}}{\gamma-1} + \frac{\bar{M}^3}{2} + \frac{1}{\gamma-1} + \frac{3}{2}\bar{M}^2\right) & \bar{c}\left(\frac{\gamma\bar{M}}{\gamma-1} + \frac{\bar{M}^3}{2} - \frac{1}{\gamma-1} - \frac{3}{2}\bar{M}^2\right) & -\bar{c}\frac{\bar{M}^3}{2} \end{bmatrix}, \tag{6}$$

and $\widetilde{E}(x) = (\gamma-1)\bar{\rho}\bar{T}\cdot\widetilde{s}(x)$, where $\widetilde{s} = C_v\cdot\widetilde{p}/\bar{p} - C_p\cdot\widetilde{\rho}/\bar{\rho}$ denotes the oscillating entropy and C_v is heat capacity at constant volume. The governing equations in (3) then become

$$[\widetilde{A}_2^+(x_h), \widetilde{A}_2^-(x_h), \widetilde{E}_2(x_h)]^T = (\boldsymbol{M^2_{w2f}})^{-1}\boldsymbol{M^1_{w2f}}[\widetilde{A}_1^+(x_h), \widetilde{A}_1^-(x_h), \widetilde{E}_1(x_h)]^T + (\boldsymbol{M^2_{w2f}})^{-1}[\widetilde{m}_n, 0, \widetilde{e}_n]^T, \tag{7}$$

where $\boldsymbol{M^1_{w2f}}$ and $\boldsymbol{M^2_{w2f}}$ are the wave to flux transfer matrices immediately before and after the resonator respectively and $\widetilde{m}_n$ and $\widetilde{e}_n$ are related to $\widetilde{A}_1^+(x_h)$ and $\widetilde{A}_1^-(x_h)$ using the HR model. As the mean flow difference before and after the HR is generally very small, $(\boldsymbol{M^2_{w2f}})^{-1}\boldsymbol{M^1_{w2f}}$ is approximately equal to an identity matrix. Substituting the full expression for $(\boldsymbol{M^2_{w2f}})^{-1}$ into Eq. (7) gives

$$\widetilde{A}_2^+(x_h) - \widetilde{A}_1^+(x_h) = \frac{\bar{c}_2}{2(\bar{M}_2+1)}\left[-\bar{M}_2 + \frac{\bar{c}_n^2(\gamma-1)}{\bar{c}_2^2(\gamma_n-1)} + (\gamma-1)\left(\frac{\bar{M}_2^2}{2} + \frac{\bar{u}_n^2}{2\bar{c}_2^2} - \frac{\bar{u}_n S_n}{i\omega V}\cdot\frac{\bar{c}_v^2}{\bar{c}_2^2}\right)\right]\cdot\frac{\widetilde{m}_n}{S_c}, \tag{8a}$$

$$\widetilde{A}_2^-(x_h) - \widetilde{A}_1^-(x_h) = \frac{\bar{c}_2}{2(\bar{M}_2-1)}\left[\bar{M}_2 + \frac{\bar{c}_n^2(\gamma-1)}{\bar{c}_2^2(\gamma_n-1)} + (\gamma-1)\left(\frac{\bar{M}_2^2}{2} + \frac{\bar{u}_n^2}{2\bar{c}_2^2} - \frac{\bar{u}_n S_n}{i\omega V}\cdot\frac{\bar{c}_v^2}{\bar{c}_2^2}\right)\right]\cdot\frac{\widetilde{m}_n}{S_c}, \tag{8b}$$

$$\widetilde{E}_2(x_h) - \widetilde{E}_1(x_h) = \frac{\bar{c}_2}{\bar{M}_2}\left[\frac{\bar{c}_n^2(\gamma-1)}{\bar{c}_2^2(\gamma_n-1)} - 1 + (\gamma-1)\left(\frac{\bar{M}_2^2}{2} + \frac{\bar{u}_n^2}{2\bar{c}_2^2} - \frac{\bar{u}_n S_n}{i\omega V}\cdot\frac{\bar{c}_v^2}{\bar{c}_2^2}\right)\right]\cdot\frac{\widetilde{m}_n}{S_c}, \tag{8c}$$

where $\bar{c}_n$ and γ_n denote mean sound velocity and heat capacity ratio in the neck, (which are set by the neck temperature) and $\gamma = \gamma_1 = \gamma_2$ denotes the constant heat capacity ratio before and after the HR. The third terms in the square brackets are all much smaller than $\bar{M}_2$ and thus can be ignored.

If the temperature in the neck is the same as that in the combustor, such that $\bar{T}_n = \bar{T}_2$ (thus $\bar{c}_n = \bar{c}_2$ and $\gamma_n = \gamma$), the entropy oscillation does not change across the HR, as $\widetilde{E}_2(x_h) - \widetilde{E}_1(x_h) = 0$ in Eq. (8c). In this case, Eqs. (8a, 8b) agree with models which assume a continuous stagnation enthalpy oscillation across the HR.[4] However, if the neck temperature is much lower than that in the combustor, which is often the case due to the cooling flow through the neck, Eqs. (8) show that both acoustic and entropy wave strength relations before and after the HR change. A test case employing the linear HR model shown in Eq. (4) is now used to show how this temperature difference affects the HR sound absorption performance. Then temperature in the HR neck is assumed equal to that in its cavity as the cooling flow is assumed to dominate the flow in the neck.

The geometry and mean flow parameters of the HR and the one-dimensional combustor are shown in Table 1. The cavity volume of the HR is set to be $2.5 \times 10^{-4}\ m^3$ thus its resonant frequency is

Table 1: Geometry and mean flow parameters of the HR and one-dimensional combustor

HR	Neck length (m)	$S_n\ (m^2)$	Cavity temperature (K)	Mean neck Mach no.
	0.005	1×10^{-4}	1000 (500)	0.01
Combustor	$S_c\ (m^2)$	$\bar{p}_1\ (MPa)$	$\bar{T}_1\ (K)$	$\bar{M}_1$
	0.031	2	1000	0.03

$\sim 535\ Hz$ for a $1000\ K$ cavity temperature and $\sim 385\ Hz$ for a $500\ K$ cavity temperature. The HR is assumed to be located at a pressure anti-node and $\widetilde{A}_1^+(x_h) = \widetilde{A}_1^-(x_h) = 100\ Pa$ are used for all frequencies. (The impact of pressure modeshapes within the combustor will be discussed in detail later). The entropy wave strength before the HR, $\widetilde{E}_1$, is assumed to be zero.

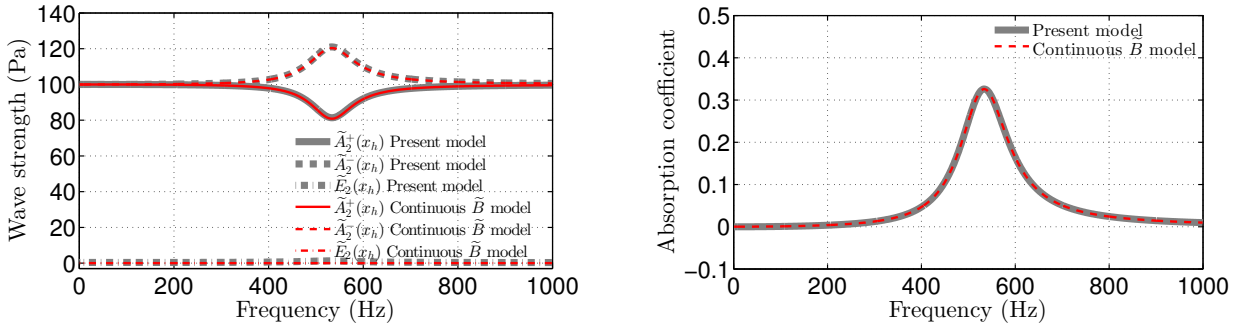

Figure 2: The wave strengths (left) and absorption coefficient (right) for the HR having a $1000\ K$ cavity.

When the HR cavity temperature matches that in the combustor, the HR is seen to affect the acoustic wave strengths near the resonant frequency, but have nearly no impact on the entropy wave strength as seen in Fig. 2(left). This is consistent with predictions from the model which assumes continuous stagnation enthalpy oscillation ($\widetilde{B}$) across the HR.[4] The two models also agree well in their prediction of the HR's sound absorption coefficient (as shown in Fig. 2(right)), defined as the absorbed energy as a fraction of the incident sound energy:[11]

$$\Delta = 1 - \frac{|\widetilde{A}_1^-|^2(1-\bar{M}_1)^2 + |\widetilde{A}_2^+|^2(1+\bar{M}_2)^2}{|\widetilde{A}_1^+|^2(1+\bar{M}_1)^2 + |\widetilde{A}_2^-|^2(1-\bar{M}_2)^2}. \tag{9}$$

When the HR cavity temperature is set to $500\ K$, less than that of the combustor, the acoustic and entropy wave strengths upstream of the HR are set to be the same as before. However, the entropy wave strength downstream of the HR is now no longer zero, due to the cold air flux oscillating through the HR neck. It can be seen in Fig. 3(left) that the strength of the generated entropy wave is strong near the resonant frequency, decreasing quickly away from it. The downstream temperature oscillation shows a similar trend (Fig. 3(right)) as it depends upon both pressure and entropy oscillations.

Thus, it can be clearly seen that the present model predicts entropy wave generations downstream of the HR which cannot be predicted by previous models that enforce stagnation enthalpy oscillation continuousness across the HR.

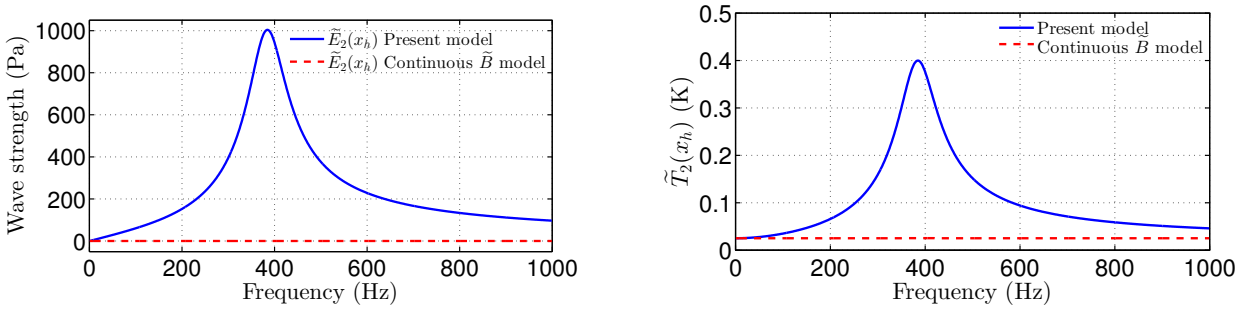

Figure 3: Entropy (left) and temperature (right) oscillations after the HR having a $500\ K$ cavity.

As well as generating an entropy wave after the HR, the lower temperature of the HR causes the relations between the acoustic wave strengths before and after the HR to also change. This follows from Eqs. (8a) and (8b), and is shown in Fig. 4(left). Similar to the acoustic wave strengths for the matched HR temperature shown in Fig. 2(left), the HR increases the upstream-propagating wave strength and decreases the downstream. Note that the present model accounts for temperature difference and predicts smaller changes than the model which assumes continuous stagnation enthalpy oscillation.[4] As a result, the peak absorption coefficient (Fig. 4(right)) from the present model is lower than that predicted by the continuous stagnation enthalpy model, with the difference disappearing gradually away from resonance.

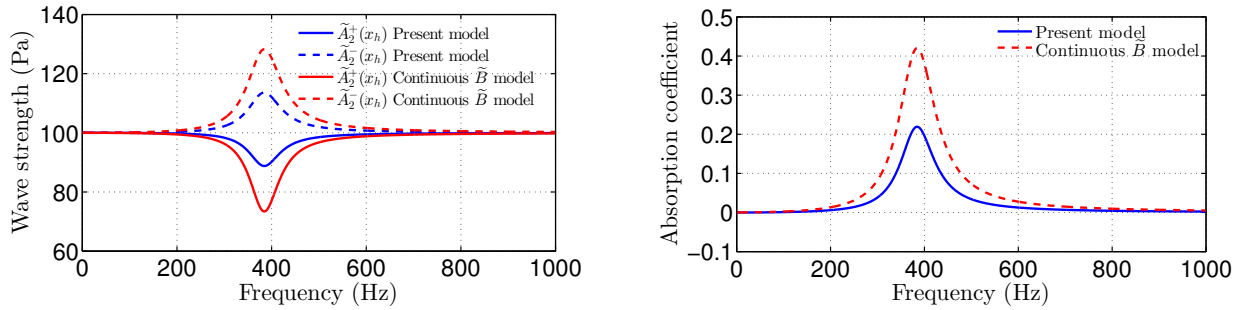

Figure 4: Acoustic wave strengths (left) and absorption coefficient (right) for the HR having a $500\ K$ cavity.

We thus conclude that temperature difference between the HR cavity and the combustor is found by the present model to generate an entropy wave downstream the HR and simultaneously change its absorption performance. This needs to be taken into account when designing HRs for a combsutor.

3. Optimizing axial distributions of multiple HRs

A Helmholtz resonator's acoustic damping performance depends on the acoustic boundary conditions of the combustor and the axial location of the HR along the combustor. We can demonstrate this via a simple example. A 1-D duct shown in Fig. 5(left) is considered , with cross sectional area $7.9 \times 10^{-3}\ m^2$, length $L = 1.5\ m$, inlet mean pressure, temperature and Mach number $101325\ Pa$, $293.15\ K$ and 0.01 respectively. A HR is attached with the same parameters in Table 1, except the cavity temperature matches the duct temperature and a cavity volume of $2.5 \times 10^{-4}\ m^3$ is chosen so that the HR resonant frequency is $296\ Hz$. Figure. 5(right) shows how the HR sound absorption coefficient depends on location, as well as its neck mouth impedance. For an open inlet, $x_h = 0.30\ m$

and $0.60\ m$ correspond to pressure anti-nodes and nodes respectively near $296\ Hz$. Thus the HR installed at the former exhibits a large absorption, while the latter exhibits nearly zero absorption.

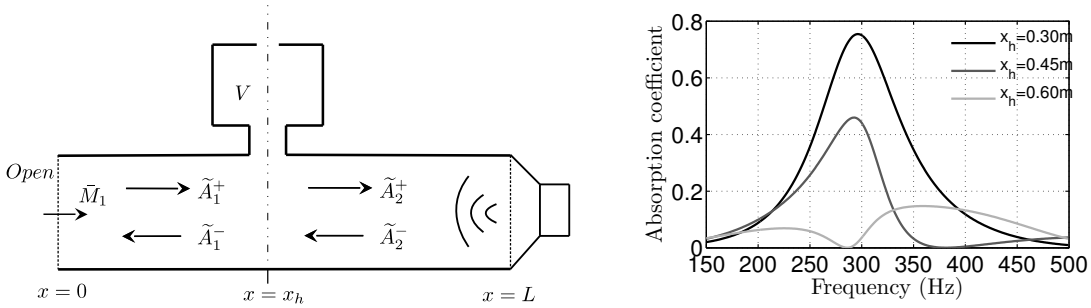

Figure 5: Schematic of duct (left) and variations of absorption coefficient with HR axial location (right).

The use of multiple HRs each tuned to a slightly different frequency offers the possibility of wider bandwidth damping than is possible with one single HR. Every HR will change the pressure modeshape along the combustor given frequency (especially near its resonant frequency), meaning that a method to optimize the locations of all the HRs simultaneously is needed. Two optimization methods are developed in this work and applied to a three-HR damping set-up in order to illustrate their use. The duct geometry, flow inlet settings and general HR parameters are the same as the case in Fig. 5. The resonant frequencies of HR1, HR2 and HR3 are tuned to $442\ Hz$, $296\ Hz$ and $150\ Hz$ respectively by adjusting their cavity volumes, with their axial locations denoted by x_{h1}, x_{h2}, and x_{h3} respectively.

Our objective is to maintain the sound absorption coefficient above a certain minimum value between the lowest and highest resonant frequencies ($[150\ Hz,\ 442Hz]$ in this case) by optimizing the HR locations. Thus, the objective function can be written as

$$\text{Min}[\Delta\ (150\ Hz \rightarrow\ 442Hz)] = F(x_{h1}, x_{h2}, x_{h3}). \tag{10}$$

3.1 Optimizing the HR locations

Two optimization procedures for locating multiple HRs are developed. One is a gradient-based method, the other a modeshape-based method. The gradient-based method assumes that distance between all neighbouring HRs is d. Assuming, for simplicity, that there are three HRs, we rename x_{h2} to x_{mid} and thus $x_{h1} = x_{mid} - d$ and $x_{h3} = x_{mid} + d$. The objective function can be simplified to $F(x_{mid}, d)$. We then search for maximum F in certain reasonable regions for x_{mid} and d (for example, $[0, 0.8\ m]$ for d and $[d, 3.5\ m]$ for x_{mid} in this case). For the duct and HRs described above, the optimum values are $x_{mid} = 0.295\ m$ and $d = 0.045\ m$ (such that $x_{h1} = 0.250\ m$, $x_{h2} = 0.295\ m$, and $x_{h3} = 0.340\ m$) with the corresponding absorption coefficient $\Delta \approx 0.39$.

The alternative modeshape-based method installs each HR at a pressure anti-node at its resonant frequency. One HR changes the modeshape at all frequencies, making it difficult to locate the pressure anti-nodes. Nevertheless, by adding the HRs to the system one by one in a specific order, this can be achieved. Considering the duct modeshape without any HRs in the example test case, the first pressure anti-node is closer to the inlet for higher frequencies than for lower ones. We thus firstly install the HR with the highest resonant frequency at the first pressure anti-node at that frequency. The HR with the next highest resonant frequency is then installed at the first pressure anti-node downstream of the first HR at its resonant frequency, accounting for the effect of the first HR on this modeshape. Then, the same procedure is repeated for subsequent HRs. For the three-HR example, the optimised HR locations are $x_{h1} = 0.194\ m$, $x_{h2} = 0.270\ m$, $x_{h3} = 0.547\ m$.

Using the optimum locations calculated by the gradient-based method which ensures a large minimum absorption coefficient, it is expected that the minimum absorption coefficient will be maintained across a wide frequency range. The modeshape-based optimisation, on the other hand, is likely

to achieve better absorption coefficients near the three resonant frequencies, but potentially at the expense of an overall low minimum absorption between resonant frequencies.

The overall absorption coefficient variation with frequency is shown in Fig. 6. The minimum overall absorption coefficient between $150\ Hz$ and $442\ Hz$ is maintained above 0.39 by the gradient-based method, and above 0.28 by the modeshape-based method, with the absorption coefficients near the first and third resonant frequencies better optimised by the latter. It should be noted that the dash-dot (color red for online) line is used here only for comparison. It has no practical meaning as it assumes that the resonators are always located at a pressure anti-node, and of course this changes with frequency.

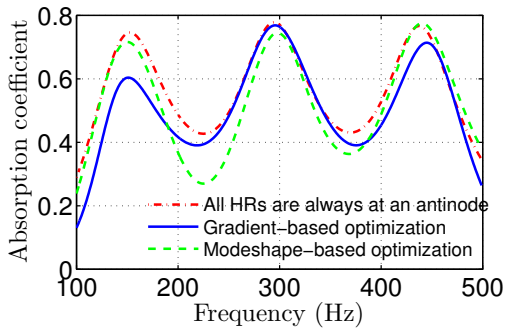

Figure 6: Overall sound absorption coefficient of the three HRs.

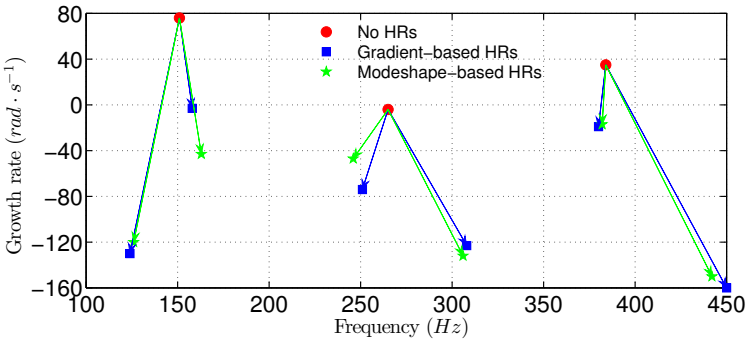

Figure 7: Eigenmodes of the Rijke tube with no HRs and with 3 HRs whose locations are optimised using two methods.

3.2 Test in OSCILOS

The three HRs and the procedure for optimising their locations are then incorporated into a Rijke tube model. For this, we use an open source combustion instability low order simulator (OSCILOS).[12,13] The combustor cross sectional area and inlet conditions match those of the cold duct considered early in section 3. The tube length is $1.5\ m$ with the flame $1\ m$ from the inlet. Then mean temperature after the flame is assumed to be 3 times that before it. The tube boundary conditions are open-open and the flame model used is the well known $n-\tau$[14] model with a first order low pass filter.

The thermoacoustic eigenmodes of this Rijke tube are calculated both with no HRs and with three HRs using the two optimisation procedures described in section 3.1 to choose their locations. These eigenmodes are shown in Fig. 7. With no HRs, three modes are seen at $(151\ Hz, 76\ rad\cdot s^{-1})$, $(265\ Hz, -4\ rad\cdot s^{-1})$ and $(384\ Hz, 35\ rad\cdot s^{-1})$ where the positive growth rates of the first and third modes indicate that these two modes are unstable. The effect of adding the location-optimised HRs is to split each of these modes into two stabilized modes. The damping effect on a specific original mode can be reasonably evaluated using the least stable of the two split modes (the other generally having a large negative growth rate meaning it can be ignored). Figure. 7 shows that these least unstable modes associated with the first $(151\ Hz)$ original mode for the gradient- and modeshape-based optimisations are $(158\ Hz, -3\ rad\cdot s^{-1})$ and $(163\ Hz, -43\ rad\cdot s^{-1})$ respectively. The lower growth rate of the latter indicates that the modeshape-based method achieves a better sound absorption performance near $151\ Hz$. Similarly, the least unstable modes associated with the second $(265\ Hz)$ original mode for the gradient- and modeshape-based HRs are $(251\ Hz, -74\ rad\cdot s^{-1})$ and $(246\ Hz, -47\ rad\cdot s^{-1})$, and those associated with the third $(384\ Hz)$ original mode are $(380\ Hz, -19\ rad\cdot s^{-1})$ and $(382\ Hz, -17\ rad\cdot s^{-1})$ respectively. The lower growth rates generated by the gradient-based multi-HRs indicate that the gradient-based method achieves better sound absorption performance near $265\ Hz$ and $384\ Hz$. These results are consistent with the absorption coefficient shown in Fig. 6.

4. Conclusion

To evaluate the sound absorption performance of a Helmholtz resonator in a real combustor, the effect of both its cavity temperature (often lower than the combustor temperature) and its location within the combustor have been studied. By combining the energy conservation equation based on stagnation enthalpy, together with the mass and momentum conservation equations, with an acoustic model for the HR, the temperature difference is found to generate an entropy wave after the HR and to simultaneously change the acoustic wave relations across the HR. Furthermore, in order to systematically choose the locations of multiple HRs, each tuned to a slightly offset frequencies, gradient-based and modeshape-based optimization methods have been developed. These aim to optimise the overall sound absorption performance over a given bandwidth. Implementation of these procedures in an open source combustion instability low-order simulator (OSCILOS) validate that they achieve this, with the gradient-based method achieving higher sound absorption between HR resonant frequencies and the modeshape-based method achieving higher sound absorption near the resonant frequencies.

REFERENCES

1. A. P. Dowling and J. E. Ffowcs Williams. *Sound and sources of sound*. John Wiley & Sons, Inc. New York, USA, 1983.
2. A. Cummings. “Acoustic nonlinearities and power losses at orifices”. In: *AIAA journal* **22**.6 (1984), pp. 786–792.
3. V. Bellucci et al. “On the use of Helmholtz resonators for damping acoustic pulsations in industrial gas turbines”. In: *Journal of engineering for gas turbines and power* **126**.2 (2004), pp. 271–275.
4. I. D. Dupère and A. P. Dowling. “The use of Helmholtz resonators in a practical combustor”. In: *Journal of engineering for gas turbines and power* **127**.2 (2005), pp. 268–275.
5. D. Zhao et al. “Acoustic damping of a Helmholtz resonator with an oscillating volume”. In: *AIAA journal* **47**.7 (2009), pp. 1672–1679.
6. M. Howe. “On the theory of unsteady high Reynolds number flow through a circular aperture”. In: *Proceedings of the Royal Society of London. A. Mathematical and Physical Sciences* **366**.1725 (1979), pp. 205–223.
7. B. Ćosić et al. “Acoustic response of Helmholtz dampers in the presence of hot grazing flow”. In: *Journal of Sound and Vibration* (2014).
8. X. Jing and X. Sun. “Experimental investigations of perforated liners with bias flow”. In: *The Journal of the Acoustical Society of America* **106**.5 (1999), pp. 2436–2441.
9. J. D. Eldredge and A. P. Dowling. “The absorption of axial acoustic waves by a perforated liner with bias flow”. In: *Journal of Fluid Mechanics* **485** (2003), pp. 307–335.
10. A. Scarpato et al. “Modeling the damping properties of perforated screens traversed by a bias flow and backed by a cavity at low Strouhal number”. In: *Journal of Sound and Vibration* **331**.2 (2012), pp. 276–290.
11. C. Morfey. “Sound transmission and generation in ducts with flow”. In: *Journal of Sound and Vibration* **14**.1 (1971), pp. 37–55.
12. J. Li, D. Yang, and A. S. Morgans. *Open Sounce Combustion Instability Low Order Simulator (OSCILOS–Long) Technical report*. Tech. rep.
13. J. Li and A. S. Morgans. “Time domain simulations of nonlinear thermoacoustic behaviour in a simple combustor using a wave-based approach”. In: *Journal of Sound and Vibration* (2015). DOI: 10.1016/j.jsv.2015.01.032.
14. L. Crocco. “Aspects of combustion stability in liquid propellant rocket motors part I: fundamentals. low frequency instability with monopropellants”. In: *Journal of the American Rocket Society* **21**.6 (1951), pp. 163–178.